EFFECT OF FUEL TEMPERATURE AND AMBIENT PRESSURE ON A COMMON RAIL RAPESEED OIL SPRAY

M.T. Bialkowski[1], T. Pekdemir[1], D.P. Towers[1], R. Reuben[1], M. Brautsch[2], G. Elsbett[3]

[1] *School of Engineering and Physical Sciences, Heriot-Watt University,*
Edinburgh, Scotland;m. Bialkowski@ hw .ac.uk
[2]*Environmental Engineering Department,University of Applied Sciences, Amberg-Weiden,*
Germany;m.brautsch@fh-amberg-weiden.de
[3]*ELSBETT Technologic GmbH, Thalmassing Germany; Guenter.Elsbett@t-online.de*

Abstract

This paper investigated spray characteristics of rapeseed oil (RSO) as renewable fuel for common-rail (OR.) diesel engines using high-speed camera image technique and Phase Doppler Anemometry (PDA). Experimental spray penetration at various injection pressures and fuel temperatures for RSO were compared with data of standard oil (SO) taken at the same varying ambient conditions. Additionally, corresponding to penetration data, data sets of spray development for these two oils were also aquired. It has been found that RSO temperature of 60°C being used in practice to preheat plant oils in modified OR, engines does not improve spray penetration to be sufficient to reach the penetration equivalent at 25°C for SO. It is concluded that producing RSO spray similar to SO one requires high injection pressure and fuel temperature, and the pressure effect is more influential. The PDA measuremens revealed stronger injection pressure effect on values of Ds2 and DID than oil temperature.

Keywords: common rail, rapeseed oil spray, spray characteristics

1. Introduction

Seeking for cleaner and sustainable fuels led into interest of using neat vegetable oils in Diesel engines. Particularly, cold pressed RSO is emerging as a potentially viable alternative to diesel fuel. Its physical and chemical properties as well as simple production and low price make it attractive source of energy. The recent studies and engine tests showed difficulties in direct fuelling Diesel engines caused by mainly by higher viscosity of RSO leading to a decrease of engine performance [15] [19] [2] [14] [4]. Despite the successful use of RSO and its derivatives in the indirect injection (IDI) Diesel engines presented by Hemmerlein [5] and in [9], similar application in the direct injection (DI) Diesel engines is still highly problematic manifesting in so-called " short-" and " long-term" problems [2] [18]. The number of successful modification of IDI engines as well as some attempts on DI ones shows that RSO can help to create sustainable and cheap source of mechanical energy. Theoretical work of modelling of plant oil atomization in DI engines has been already performed [17]. The latest development of common-rail engines indicates the high performance and efficiency together with deep emission reduction. It can be expected that modifications of the common-rail injection system would enable it to operate on RSO and hence create very efficient and sustainable diesel powered energy source. Nevertheless recent operating of the common-rail on RSO is problematic due to different physical properties of this oil badly influencing fuel delivery, spray development and reducing the creation of air/fuel mixture. The long-term problems manifest in cooking tendencies and carbon deposit formation [2]. The CR injection process finely controlled by an electronic control unit does not overcome spray obstruction and therefore needs to be redesigned. To improve atomization the injection system requires modification derived from fundamental spray pattern characteristics, droplet sizing tests and careful engine tests. In order to improve

atomization of RSO parameters like penetration, spray cone angle and drop size distribution under different injection fuel pressure and temperature needs to be assessed similarly to studies performed for diesel in [8][11][1][13] or its alternative [12]. Such studies could provide the necessary basic experimental data to characterize the mechanism responsible for deficiency during RSO combustion in CR engines.

The study of RSO spray characterization is a part of the ongoing project on the modification of CR injection system including injection and engine test of a Mercedes common rail car. As a final output a modified CR engine full-filing EURO IV criteria is expected to be achieved.

2. Experimental details

Studies of spray penetration and spray droplet sizing were performed under several injection and ambient conditions. Rape-seed oil and calibration oil named here as standard oil were used in experiments at different oil temperatures. In all experiments the duration of injections was 1 ms to minimize small drop entrainment inside the chamber during the injection set.

2. 1. Injection chamber

All the measurements were made in a high-pressure injection chamber which enabled to study the spray behavior at different injection conditions. The high-pressure const ant-volume chamber was manufactured at Heriot-Watt University and employed three high-quality borosilicate windows of the dimensions of 175 mm (two end ones) and 48 mm (side one), and a injector port mounted on the upper face on the chamber. Location of the the injection port shown "schematically" in Figure 1 and was designed to accommodate a commercial, seat-hole Mercedes (A6110700587) common-rail injector. The tip of the injector was set to produce a single, vertical spray-jet by selecting one of the six holes of the injector, while rest of those were still operating. Two different gases were used in the experiments allowing to reproduce in-engine air compression conditions (N_2, SF_6) up to maximum pressure equivalent to 4.9 MPa of air. Prior to the measurements, the gases were pumped in the chamber which had been emptied with a vacuum pump. The pressure in the chamber were controlled by in-line valves and the gases were entrained through a system of spray devices. The gas in the chamber remained still and was replaced after each consecutive set of injections to avoid fuel build up and contamination of the windows.

2.2. Injection system and auxiliaries

The Bosch CR system was applied to raise the fuel pressure up to 1500 bar however the pressure up to 1350 bar was utilized in the experiments. Injection pressure was controlled by the pressure control valve powered by a linear switching power supply (DPS4005). The pressure rail supplies fuel to four injector ports, three of which were blocked off. The effective fuel pressure was read from the pressure sensor by converting an output voltage according to a calibration formula. The pressure rail bar and the injector were equipped with a separate heating control system with accuracy of ± 2.5°C. Temperature readings of fuels in a tank, fuel lines, rail and nozzle body was controlled by three independent heating/cooling loops. Prior to each experiment the fuel inlet pipeline was heated up and flushing through with a fuel at test temperature. The excessive fuel flow was returned to a fuel tank being cooled by a set of heat exchangers. The injection was activated by a commercially available Common Rail Signal Unit (Hartridge HK850) to produce a

single injection pulse. Both fuels were injected at a rate of 1 Hz and duration of 1 ms throughout the tests. Table 1 lists full injection conditions and experimental parameters and some properties of used oils.

2. 3. Measurement technique

2.3.1. Spray visualization

A Kodak high-speed image analyzer (HSC) - model 4540hx was used to capture images of spray produced over a range of injection conditions. Recording frame rates were adjustable and 9000 frames per second at progressively reduced resolution and framing area were set allowing the entire injection phase to be recorded. To enable a view of the development of a single spray a single source of white halogen floodlight with a diffuser was applied.

Table 1. Fuel properties and injection condition

Fuel type	Standard oil	Rape-seed oil
Density at 20°C[kg/m^3]	823.2	921.1
Viscosity at 20°C[mm^2/s]	3.81	73.78
Fuel temperature [°C]	25, 40, 60	
Fuel injection pressure [MPa]	56.3, 131.3	
Fuel pre-pressure [bar]	4.1	
In-cylinder temperature [°C]	20	
In-cylinder densities [kg/m^3]	5.94, 14.94, 59.96	
Injection frequency [Hz]	1.0	

The high-speed camera was brought to focus using a specially designed nozzle sleeve. To record a full view of a single spray, the setup shown in Figure 1 was used. For calibration purpose some images of a millimeter scale in focus were taken and used in further processing. The exposure of a single frame was 0.11 ms resulting with the uncertainty due to spray development during the exposure of ±3 mm. It was found that during the early stages of injection the spray penetration yields in a length varied by 3 mm. The injection pulse sent from the injector activator triggered off the camera. After correction for optical distortion, five sets of photographs were taken for each of the three different injection pressures. The procedure was repeated for different chamber pressures and fuel temperatures. Because the tip of the nozzle was not visually accessible through the nozzle cover, the beginning of the injection was worked out based on acquired trigger signal.
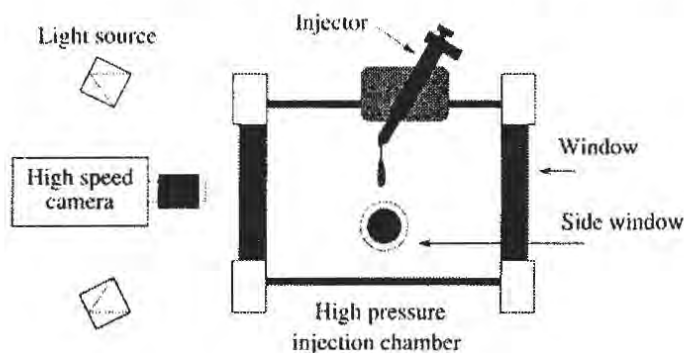

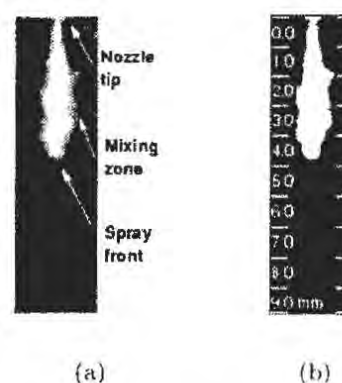*Figure 1. High speed camera set-up view (not scaled).*

(a)   (b)

Figure 2. (a) Spray structure; (b) Image of a thresh- olded spray

Gamma correction of the images prior to the technique of a threshold value was applied. Outlining the spray from the background employed a threshold processing similar to [16]. The optimal threshold level was chosen by analyzing images from each data set and results of the numerical analysis of a modified image. The spray penetration data was obtained from a numerical processing of threshold converted and cropped spray image. In all cases the maximum penetration values represent distances of the furtherest drops in the spray front correlated according to the threshold level and corrected by a spray length present in the nozzle cover. The processing employed open-source image processing software as well as their own written processing scripts. A sample of the original spray image together with a processed one are shown in Figure 2. The calculated values of spray penetration were found to be slightly dependent on the threshold level. Threshold variation of 15 % yielded in up to 4 % change in measured penetration. However, spray images taken from the same injection can have pulse-to-pulse variation because of various reasons. Hence the spray penetration obtained was averaged. Also, the coverage of the nozzle tip, camera shakes and lamp positioning could produce some errors.

2.3.2 Spray droplet sizing

The experimental PDA optical set-up is shown in Figure 3. The injection parameters was the same as shown in Table 1. The measurement for each injection and ambient condition was repeated 3 times at the same point for 7 consecutive injections. Measurement of Sauter mean diameter was performed for both RSO and SO. The final presentation was based on the averaged drop population. The light source was an Argon-Ion Dantec laser providing beams at two wavelengths, green (λ=514.5 nm) and blue (λ=488.0 nm). The beams were transmitted to the PDA probe through an optical fibre and then focused at the measurement volume at a focal length of 600 mm from the PDA transmitter and 30 mm downstream from the nozzle tip. A measurement volume was located in the centreline of the spray with the maximum deviation form the centreline of ± 1mm. The centreline of a spray was found by scanning of spray velocities in X,Y and Z direction. The PDA transmitter was positioned at an angle of 4°. The receiving optics was located at 310 mm from the measurement volume at 21°. Hence the PDA system was operating at the scattering angle of 25°. The alignment, focus of the PDA and validation of the measurements were checked with a water nebuliser resulting in a droplets spectrum of Sauter mean diameter of ~10μm.
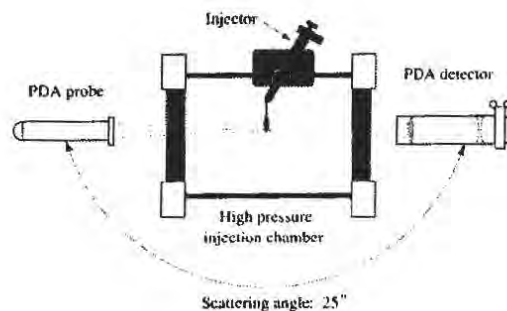

Figure 3. Representation of the setup for PAD measurement.

Prior to the spray measurements the system required calibration to chose suitable photomultipliers (PMT) voltage and the validation level. The sensitivity of the PMT was finally set to 1000 V whereas the voltage for successful completion of the test varied between 900 V and 1200 V. Randomly at 1000 V the PDA signal got saturated and it was

necessary to destabilize the PMT. A summary of PDA setup is presented in Table 2. It needs to be stressed that measurements of dense sprays of SO and RSO remain very difficult and some of the errors are difficult to reduce and unavoidable. All the sizing test were performed using two dimensional PDA setup, whereas the raw data processing was carried out with ID configuration only due to better validation and proper statical presentation of the drop populations similarly to the method of a dense spray analysis performed by Lacoste et al. [10].

Table 2. Parameters of the PDA setup

Beam separation [mm]	25
Fringe spacing [μ]	12.350 11.714
Number of fringes	12
Velocity bandwidth [m/s]	-37.0 to 111.1
Maximum diameter [μ]	178.82
Particle/medium refractive index	1.41-1.47/1
Validation level [dB]	-3
Max. spherical deviation [%]	15

Table 3. Distribution ranges

	size [μm]		size [μm]
A	0.00-3.58	K	35.76-39.34
B	3.58-7.15	L	39.34-42.92
C	7.15-10.73	M	42.92-46.49
D	10.73-14.31	N	46.49-50.07
E	14.31-17.88	O	50.07-53.65
F	17.88-21.46	P	53.65-57.22
G	21.46-25.04	Q	57.22-60.80
H	25.04-28.61	R	60.80-64.38
I	28.61-32.19	S	64.38-67.95
J	32.19-35.76	T	67.95-71.53

3. Results and discussion

3. 1. Spray penetration results

Spray penetration lengths were measured for injection pressures of 56.3 and 131.1 MPa and three different fuel injection temperatures: 25, 40 and 60°C, and chamber densities in the range from 5 to 60 kg/m^3. The chamber temperature was kept constant at 20°C throughout experiments. The results of measurements of RSO were compared with the SO spray at 25°C. Processing of the spray development images showed discrepancy between the solenoid valve activation and injection rate. Playback of an image sequence presented time delay between time when the injection signal activated the high-speed camera and the first sight of fuel appearing at nozzle tip as previously found in [11]. This phenomenon was noted for all the injection rates of tested fuels however the delay phenomenon was longer for RSO. Higher viscosity of RSO results in slower flow within feed passages and therefore higher "hesitation" . In case of low injection pressure (~300 bars) and fuel temperature injection did not result in atomization at all. The penetration data shown in this paper are referenced from the time the injector is activated.

As can be seen from Figure 4 through 5 that peneration of RSO spray was poorer in

57

comparison to SO. Spray processing revealed differences in the shape and rate of development of RSO sprays, therefore the results presented have been derived from the injection for comparative analysis. The figures and images presented here are limited to a few examples of a larger set of experimental data. Average spray data penetration with respect of time are graphically presented for SO and RSO. Additionally, for two different injection system of 56.3 and 131.3 MPa the penetration data are presented together with sequences of images presenting spray development at ambient pressure of 4.9 MPa and 1.4 ms after the nozzle was energized. For each injection pressure of 56.3 and 131.3 MPa, a set of three graphs corresponding to three different ambient pressures of 0.5, 1.2 and 4.9 MPa are presented.

It can be seen that temperature increase has some effect on spray development resulting in an increase of penetration due to a reduction of RSO viscosity. Although, the RSO oil spray penetration at 60 °C was observed to be slower than that of SO at 25 °C for all the pressure conditions investigated. Figures 4(a) and 4(b) represent the liquid spray developing at the lowest and the moderate ambient pressure employed. It can be seen that penetration at ambient pressure of 0.5 MPa is more effected by temperature, whereas the effect of ambient pressure at 1.2 and 4.9 MPa temperature effect is less pronounced, Figures 4(b) and 4(c), resulting in flatter curve slopes and closer location of the penetration curves for the RSO. Noticeable similarity in the curve trends between 1.2 and 4.9 MPa can be seen. Also it can be found that the spray penetration curves are approximately linear with time in the earlier stages of the injection i.e. before $12 \cdot 10^{-4}$ s. It was observed from spray images that increased ambient pressure results in significant reduction of penetration and "richer" and denser fuel spray. Some typical spray images corresponding to 4.9 Map of amient pressure are shown in Figure 4(d). It can be clearly seen from the Figure 4(d) that increase temperature results in fuller spray with longer penetration. The front edge of the sprays appears to be more rounded and slightly demonstrates sign of conical shape as the whole spray becomes more symmetrical. Air entrainment in this case remains low and periphery of the sprays is smooth. The aerodynamic interaction between spray and ambient gas is negligible due to relatively low injection pressure and the high ambient gas density ($\rho=59.96$ kg/m^3).
It can be conculed from the data presented in these figures that lower ambient pressure, higher injection pressure and higher fuel temperature render RSO spray characteristics similar to that of SO.

High injection pressure (131.3 MPa) results in the penetration rates increasing rapidly. The spray penetration under a higher injection pressure is faster than under a lower injection pressure (56.3 MPa) for both types of oil under same ambient conditions. Figures 5(a,b) and 5(c) present the higher values of spray penetrations achieved in the presented study for each set of ambient conditions. The data indicates that temperature has got some degree of effect on the spray penetration. But the effect is not significant and does not follow an expected trend of an increase with increased temperature. The injection pressure effect is more significant and similar to one reported in [8] performed in the similar range of the injection conditions. It can be concluded that in this case the pressure drop across the nozzle is less affected by changes of RSO viscosities and more by momentum forces resulting in penetration values less dependent on temperature. The SO values indicate shorter injection delay and in all cases the first detected spray was recorded before $5 \cdot 10^{-4}$ s. The same trend cannot be observed clearly for RSO. Increased injection pressure slightly reduces injection delay as it was concluded before this does affect the fuel flow inside the nozzle.
Spray changes presented in Figure 5(d) show that higher injection pressure makes the leading edge of the sprays more distorted. It indicates the higher degree of air entrainment and presence of small vortexes at the edge of the sprays. The presence of turbulence
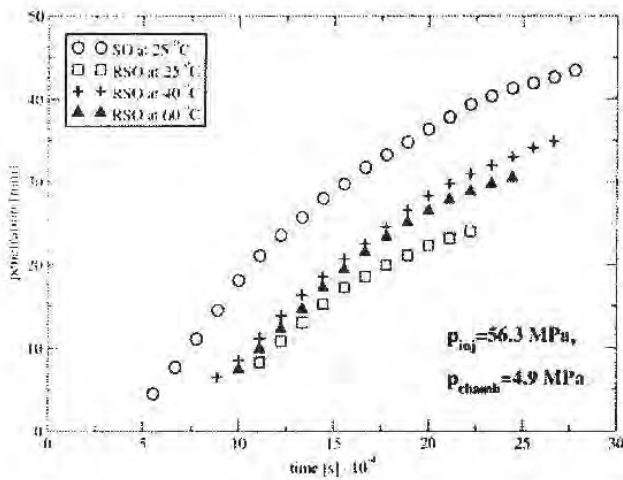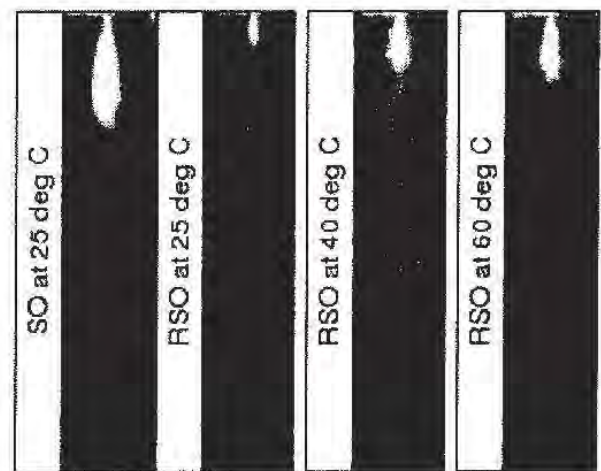
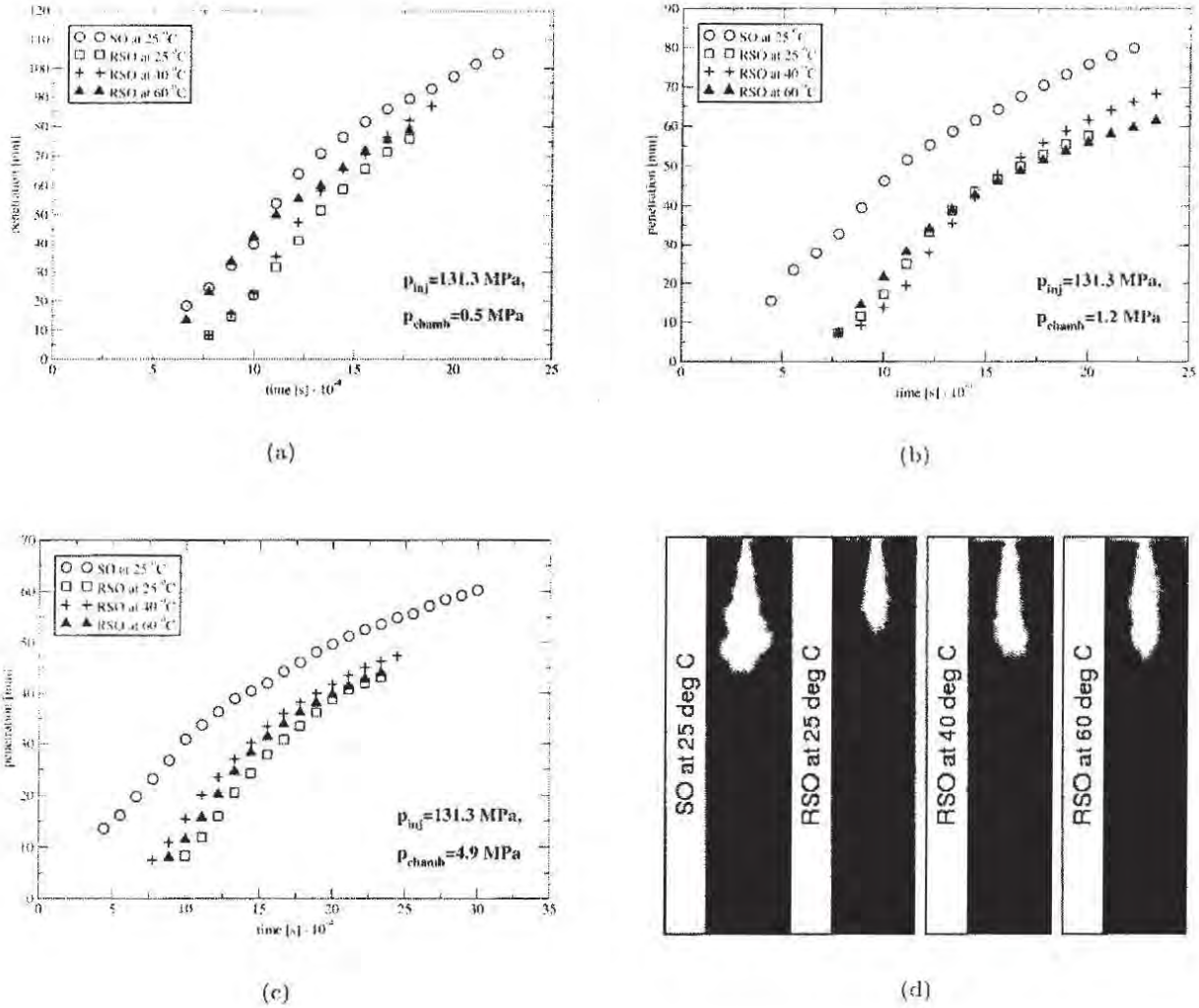indicates a "blunt" edge along a spray.
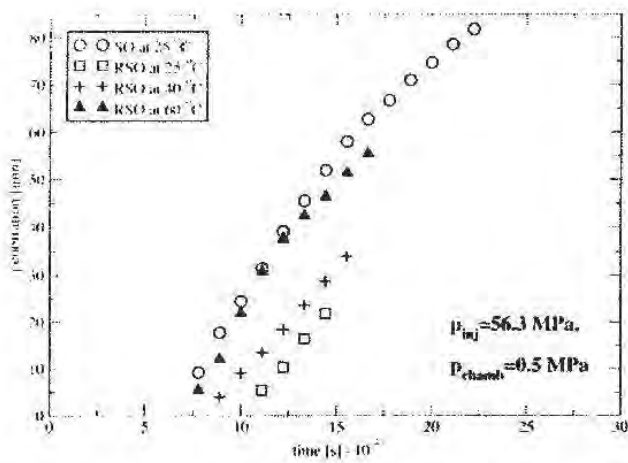
(a)
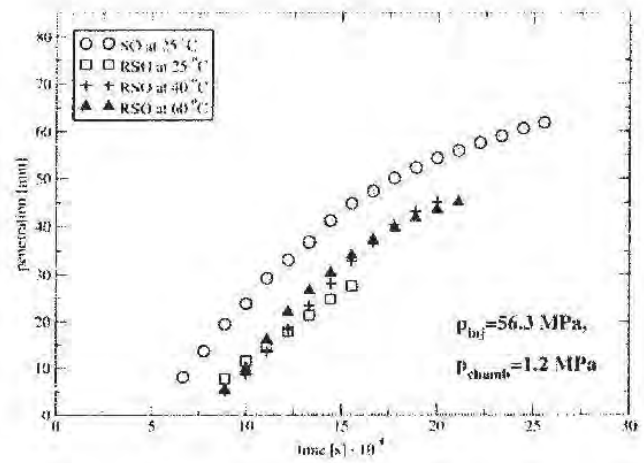
(b)

(c)

(d)

Figure 4. Comparison of penetration rate for standard and rapeseed oil for injection pressure of 56.3 MPa and ambient pressure of (a) 0.5 MPa, (b)1.2 MPa and (c)4.9 MPa.(d) Spray images of standard and rapeseed oil at 1.4 ms after nozzle was energised for injection pressure of 56.3 MPa and ambient pressure of 4.9 MPa

Shear forces between the stagnant gas and liquid sprays results in such phenomenon which would contribute in increasing mixing and evaporation of RSO droplets as concluded previously by Laguitton et al. [11]. Comparison of Figure 4(d) and 5(d) shows clear effect of the increasing injection pressure as a main force for enhanced spray development as this effect can be easily expected.

The spray penetration result obtained from image processing are not easily adjustable to known correlations describing the spray penetration. A two-zone penetration model based on jet instability analysis as proposed by Hiroyasu and Arai [6] in which a period before breaking-up can be neglected has not provide satisfactory agreement with the experimental results even for adjusted constants. Different approach to correlate experimental results presented in [7] including the injection mean velocity showed slightly better agreement however deviation of the experimental and correlated penetration values was still too high (~120% on average). It is expected that existing correlations would require further modification taking into account high viscosity and surface tension of RSO as well as detailed nozzle geometry.

3. 2. Droplet sizing results

Samples of the PDA measurements for RSO taken at 30 mm from the nozzle tip are presented in a form of Sauter (D_{32}) and arithmetic (D_{10}) mean diameters and compated with SO. Some selected distribution curves for the RSO are shown. It needs to be highlighted that the PDA measurements was effected by number or "satellite" drops present closely to the measuring point. These drops were detected during the high speed imaging experiments and might lead to the higher number of big drops present in nearly each drop population.

(a)

(b)

(c)

(d)

Figure 5. Comparison of penetration rate for standard and rapeseed oil for injection pressure of 131.3 MPa and ambient pressure of (a) 0.5 MPa, (b)1.2 MPa and (c)4.9 MPa.(d) Spray images of standard and rapeseed oil at 1.4 ms after nozzle was energised for injection pressure of 131.3 MPa and ambient pressure of 4.9 MPa

This occurred mainly while SO was used in experiments. Close analysis of the injection pictures showed also presence of circulating drops inside vortexes appearing especially at the edge of sprays. Such phenomenom was likely observed for SO than for RSO. PDA tests of RSO sprays revealed already reported [10] difficulties in attaining measurements in the dense spray environment. Figure 6 (a) presents the variation of the arithmetic mean diameter for RSO taken at different ambient pressures with injection temperature at constant injection pressure of 56.3 MPa. It can be seen that the average size increases with an increase in ambient pressure (gas density) for all injection temperatures. The similar observation was reported in [3] and it can be explained as the result of reduction of the relative velocity and hence tendency to drops breakup. The aerodynamic resistance of the ambient gas has

60

important role in breaking-up the RSO drops while the oil is characterized by high surface tension and viscosity. Lower ambient pressure enhances spray velocity and therefore more readily small drop formation. In Figure 6 it can be clearly seen that the mean drop size is less effected by the oil temperature than by the injection pressure in a form of nearly constant slope of a linear relation. In both cases of low and moderate ambient pressure (0.5 and 1.2 MPa), the mean drop size tends to decrease with temperature, however this tendency is rather weak. For ambient pressure of 4.9 MPa the arithmetic mean diameter does not vary noticeably and its linear presentation remains almost constant. It can be concluded that such observation is caused by negligible effect of surface tension and viscosity changes with temperature in comparison with the aerodynamic resistance of the ambient gas. Furthermore, the actual oil temperature leaving the nozzle tip can be lower from the temperature in the oil delivery line. Despite of frequent flow of oil through the nozzle and its careful insulation, heat losses in that system are inevitable.

Figure 6(b) provides similar analysis of the arithmetic mean diameter for the RSO at higher injection pressure. As it can be expected the curves express the similar trend to those recorded for 56.3 MPa, but result in smaller arithmetic mean diameters. The D_{10} values seem to correlate with the temperature better that in case of lower injection pressure. The slopes decrease with an increase of the RSO temperature. Furthermore, the recorded values are lower than these presented in Figure 6(a). As result of higher injection pressure the spray velocity overcomes the disruptive aerodynamics forces and more likely causes the secondary break-up of drops. This is clearly observed for curves showing results taken at ambient pressure of 0.5 and 1.2 MPa. Values of the D_{10} at 4.9 MPa are close to those recorded for the same ambient pressure in Figure 6(a). Again, the effect of the aerodynamic resistance of the ambient gas balanced by the spray motion is more pronounced even for the injection pressure more than two times higher.

Figures 7(a) and Figures 7(b) show a different presentation of the droplet size variation but using the Sauter mean diameter. As a compilation of the previous data used in calculation of the D_{10} plots it can be expected that the presented values follow the same trend for the different ambient pressure as well as for the different temperatures but their values are significantly higher. Similarly it can be seen that the effect of temperature is pronounced for the highest ambient pressure and shows more rapid decrease for the injection of 131.3 MPa.

It is interesting to compare some of the D_{32} and D_{10} values for RSO with these obtained for SO. Brief evaluation shows that for injection pressure of 131.3 MPa and oil temperature of 30 °C values of D_{32} and D_{10} are not different from the RSO one at the same temperature. For instance for SO and at 56.3 MPa D_{32}=54.03 μm and D_{10}=17.37 μm. Same analysis of D_{32} and D_{10} at 131.3 MPa follows the same tendency. In this case the D_{32} and D_{10} are 34.60 μm and 15.20 μm respectively. Summary of the variation of the droplet size is presented in Table 4.

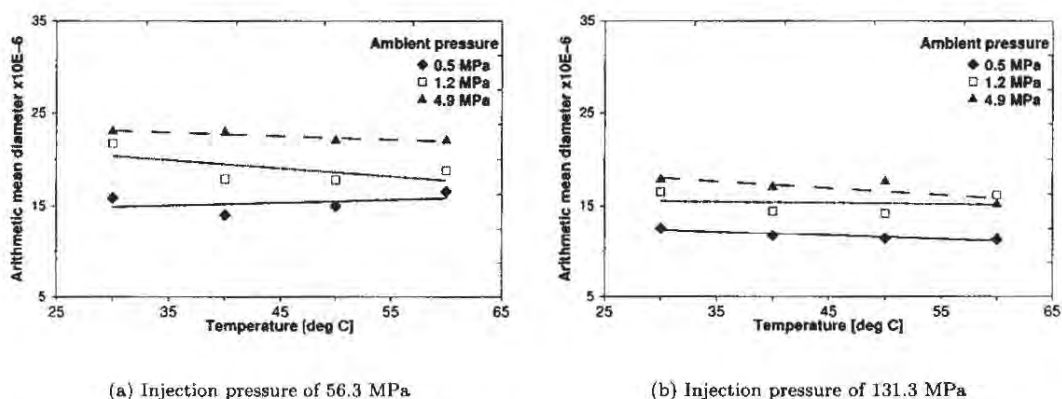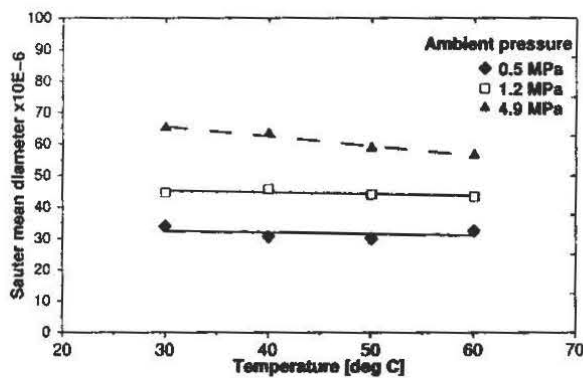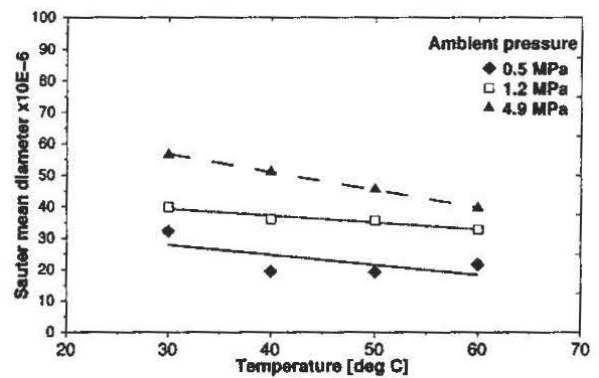(a) Injection pressure of 56.3 MPa   (b) Injection pressure of 131.3 MPa

Figure 6. Effect of temperature and ambient pressure on the arithmetic mean diameter, D_{10}.

Samples of RSO distribution for the injection pressure of 56.3 and 131.3 MPa are presented in Figures 8 to 10 for different ambient pressures of 0.5, 1.2 and 4.9 MPa. Series of drop size ranges placed on X-axis are given in Table-3. The distributions of droplet size are broad and show generally only one pick. In all cases a drop population is presented by means of the average distribution curve for strictly cooperative reason. These graphs supplement previous presentation of D_{32} and D_{10} and should be carefully interpreted. Each graph consists of 3 curves representing 3 different oil temperatures. In all cases effect of injection temperature does not follow expected trend. Temperature has less effect on distribution than injection pressure. Figures 8(a,b) shows that higher injection pressure results in higher number of drops within smaller ranges which correlates with presented values of D_{32} and D_{10} in Figures 6 and 7 for 0.5 MPa. By increasing the ambient gas pressure (Figure 9) the distribution curve shifts more towards higher drop ranges. Effect of injection pressure is similar to that in Figures 8-10.

At high ambient gas pressure of 4,9 MPa (Figure 10), drop population consists of high number of small drops as well as significant number of bigger ones (ranges from L-S). Contribution of these big drops in values of D_{32} and D_{10} is significant, thus the increased number of small drops does not result in reduced values of mean drop diameters since the noticeable number of big drops is present in the population. Explanation of presence of the big drops at higher injection pressure is quite difficult.
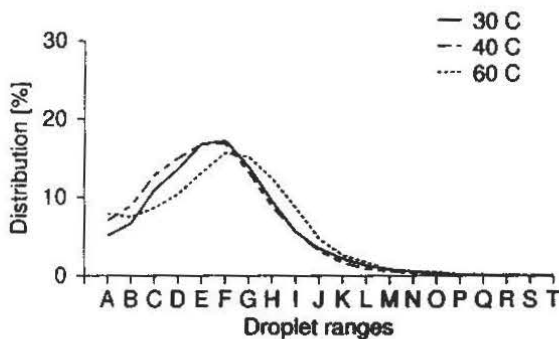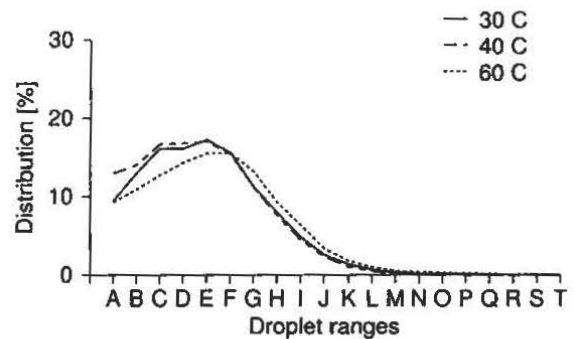

(a) Injection pressure of 56.3 MPa   (b) Injection pressure of 131.3 MPa

Figure 7. Effect of temperature and ambient pressure on the Sauter mean diameter, D_{32}
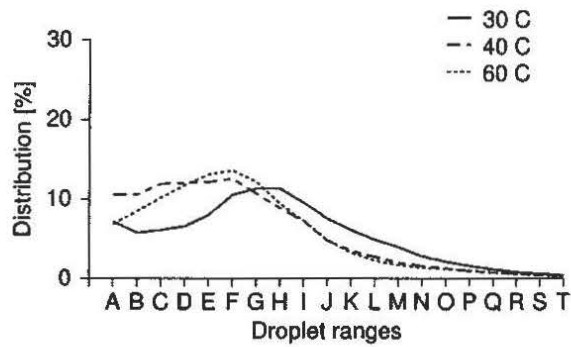

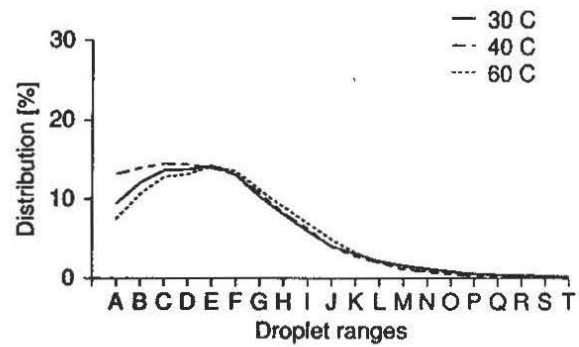(a) Injection pressure of 56.3 MPa   (b) Injection pressure of 131.3 MPa

Figure 8. Droplet diameter distribution of the RSO at ambient pressure of 0.5 MPa at various injection temperatures.
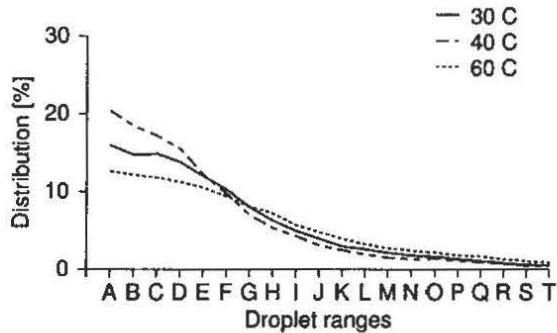
(a) Injection pressure of 56.3 MPa

(b) Injection pressure of 131.3 MPa

Figure 9. Droplet diameter distribution of the RSO at ambient pressure of 1.2 MPa
at various injection temperatures.

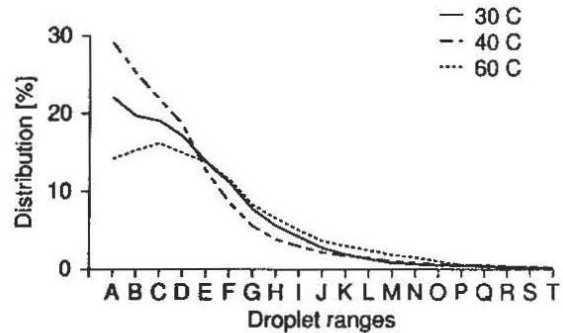(a) Injection pressure of 56.3 MPa

(b) Injection pressure of 131.3 MPa

Figure 10. Droplet diameter distribution of the RSO at ambient pressure of 4.9 MPa
at various injection temperatures.

An earlier study [10] indicates droplet diameters of diesel fuel up to 500 μm for much lower injection pressures. Such dense spray of RSO especially at high injection pressures may exhibit tendency to drop coalescence during interaction in dense atmosphere of the injection volume. As penetration length increases viscosity of RSO dramatically drops down to ambient temperature and even at high injection pressure the effect of viscosity on the mean diameter remains still superior as it was shown by Tabata et al. [20]

Table 4. D_{10}, D_{32} of standard and rapeseed oil(at ambient pressure of 1.2MPa

	Standard oil		Rape-seed oil	
Injection pressure [MPa]	56.3	131.3	56.3	131.3
D_{10} [μm]	17.37	15.20	22.34	17.21
D_{32} [μm]	54.03	34.60	45.48	40.04

4.   Conclusion

In this paper a study of rape-seed oil spray was made and a comparison of penetration and mean drop diameters with standard oil was performed. The experimental analysis of the spray characteristics has led to the following conclusions:

1. The penetration profiles were shown to be more dependent on injection pressure than oil temperature at high ambient pressures. Rape-seed oil temperature of 60°C does not improve spray penetration to be sufficient to reach the penetration equivalent at 25 °C for standard oil.

2. RSO sprays penetration is slower than for SO and sprays have a conical shape. The spray leading edge becomes more rounded and the spray becomes shorter and denser with increases in ambient pressure.

3. Higher injection pressure produces smaller Sauter and arithmetic mean diameter. Similarly to penetration results, the mean drop size diameters are more dependent on injection pressure than injection temperature.

4. Values of D_{32} and D_{10} for rape-seed oil at 30 °C and standard oil are very similar.

5. PDA measurements of a rape-seed oil spray manifest some difficulties typically accounted for dense sprays. Validation of the PDA result should be performed using another sizing technique.

5. Acknowledgements

References

[1]   Bae C., Kang J., and Lee H.; Diesel spray development from vco nozzle with common-rail. *2001 Fall Technical Conference*, 2001.

[2]   Elsbett Company. Private communications.

[3]   M S El-Beshbeeshy, J T Hodges, and M L Corradini. Image analysis of diesel sprays. *SAE*, 1992.

[4]   He Y. and Bao Y. D.; Study on rapeseed oil as alternative fuel for a single-cylinder diesel engine. *Renewable Energy*, 2003.

[5]   Hemmerlein N., Korte V., and Richter H.; Performance, exhaust emissions and durability of modern diesel engines running on rapeseed oil. *SAE Transactions*, 1991.

[6]   Hiroyasu H. and Arai M.; Fuel spray penetration and spray angle in diesel engines. *Trans. SAE Japan*, 1980.

[7]   Jimenez J., Mendez Z., Castro F., Tinaut F. V. and Gimenez B.; Experimental comparison between conventional and bio-derived fuel sprays. *SAE*, 2001.

[8]   Kennaird D. A., Crua C., Lacoste J., Heikal M. R., Gold M.R. and Jackson N.S.; In-cylinder penetration and break-up of diesel sprays using a common-rail injection system. *SAE*, 2002.

[9]   Not known. Filtered used frying fat powers diesel fleet. *JAOC*, 1982.

[10]   Lacoste J., Kennaird D., Begg S. and Heikal M. R.; Phase doppler anemometry measurements of a diesel spray. *Not reported*, Not reported.

[11]   Laguitton O., Gold M., Kennaird D., Crua C., Lacoste J. and Heikal M.; Spray development and combustion characteristics for common-rail diesel injection systems. In *IMechE Conference on Fuel Injection Systems*, 2002.

[12]   Lee C. S. and Reitz R. D.; Effect of liquid properties on the breakup mechanism of high-speed liquid drops. *Atomisation and Spray*, 2001.

[13] Lee K. and Reitz R.; Investigation of spray charasteristics from a low-pressure common rail injector for use in homogenous charge compression ignition engine. *Measurement Science and Technology*, 2004.

[14] McDonnell K., Ward S., Leahy J. J. and McNulty P.; Properties of rapeseed for use as diesel fuel extender. *JOACS*, 1999.

[15] McDonnell P. K., Ward S. M., McNulty P. B. and Howard-Hildige R.; Results of engine and vehicle testing of semirefined rapeseed oil. *Transactions of the ASAE*, 2000.

[16] Morgan R.. Wray J., Kennaird D. A.. Crua C. and Heikal M. R.;The influence of injector parameters on the formation and break-up of a diesel spray. *SAE*, 2001.

[17] Msipa C.K.M.. Goering C.E. and Karcher T.D.; Vegetable oil atomisation in a DI diesel engine. *Transactions of the ASAE*, 1983.

[18] Nwafor O.M.; The effect of elevated fuel inlet temperature on performance of diesel engine running on neat vegetable oil at constant speed conditions. *Renewable Energy*, 2003.

[19] Peterson C.L.. Wagner D.L. and Auld D.L.; Vegetable oil substitutes for diesel fuel. *Transaction ASAE*, 1983.

[20] Tabata M. and Arai M.; Atomization of high viscosity liquid by a diesel nozzle. *Bulletin of JSME*, 1986.